Proc. Natl. Acad. Sci. USA
Vol. 95, pp. 3960–3965, March 1998
Neurobiology

staggerer phenotype in retinoid-related orphan receptor α-deficient mice

MARKUS STEINMAYR*, ELISABETH ANDRÉ*, FRANÇOIS CONQUET*, LAURE RONDI-REIG†, NICOLE DELHAYE-BOUCHAUD†, NATHALIE AUCLAIR‡, HERVÉ DANIEL‡, FRANCIS CRÉPEL‡, JEAN MARIANI†, CONSTANTINO SOTELO§, AND MICHAEL BECKER-ANDRÉ*¶

*Geneva Biomedical Research Institute, Glaxo Wellcome Research and Development S.A., 4, chemin des Aulx, 1228 Plan-les-Ouates, Switzerland; †Laboratoire de Neurobiologie du Développement, and ‡Laboratoire de Neurobiologie et Neuropharmacologie du Développement, Institut des Neurosciences, Bâtiment B, Université Pierre et Marie Curie, 7, Quai Saint-Bernard, 75252 Paris Cedex 05, France; and §Hôpital de la Salpetrière, Institut National de la Santé et de la Recherche Médicale, U 106, 47, Boulevard de l'Hôpital, 75651 Paris Cedex 13, France

Communicated by William T. Greenough, University of Illinois, Urbana, IL, December 22, 1997 (received for review September 15, 1997)

ABSTRACT **Retinoid-related orphan receptor α (RORα) is a member of the nuclear receptor superfamily. To study its physiological role we generated null-mutant mice by targeted insertion of a *lacZ* reporter gene encoding the enzyme β-galactosidase. In heterozygous RORα$^{+/-}$ mice we found β-galactosidase activity, indicative of RORα protein expression, confined to the central nervous system, skin and testis. In the central nervous system, the RORα gene is expressed in cerebellar Purkinje cells, the thalamus, the suprachiasmatic nuclei, and retinal ganglion cells. In skin, RORα is strongly expressed in the hair follicle, the epidermis, and the sebaceous gland. Finally, the peritubular cells of the testis and the epithelial cells of the epididymis also strongly express RORα. Recently, it was reported that the ataxic mouse mutant *staggerer* (*sg*/*sg*) is caused by a deletion in the RORα gene. The analysis of the cerebellar and the behavioral phenotype of homozygous RORα$^{-/-}$ mice proves identity to *sg*/*sg* mice. Although the absence of RORα causes dramatic developmental effects in the cerebellum, it has no apparent morphological effect on thalamus, hypothalamus, and retina. Similarly, testis and skin of RORα$^{-/-}$ mice display a normal phenotype. However, the pelage hair of both *sg*/*sg* and RORα$^{-/-}$ is significantly less dense and when shaved shows reluctance to regrow.**

Nuclear receptors form a structurally related superfamily of ligand-activated transcription factors (1). They are involved in several aspects of vertebrate physiology, such as development and homeostasis. Important examples are the steroid hormone receptors that regulate, in a ligand-dependent manner, specific sets of responding genes. The retinoid-related orphan nuclear receptor (ROR) α (2, 3), RORβ (4), and RORγ (5) constitute a subfamily of nuclear receptors that bind to DNA both as monomers and dimers. Distribution of RORα mRNA suggests that this receptor is widely expressed and functions in several organs including brain, heart, liver, lung, and testis; highest levels were found in peripheral blood leukocytes and skin (M.B.-A., unpublished data). RORα exists in four splicing isoforms: RORα1–4. They display different N-terminal domains causing different DNA binding site preferences (3), and they display differential expression profiles: in the thalamus there is only RORα1 mRNA; RORα4 (=RZRα) (2) transcripts are predominant in leukocytes and skin; RORα2 and RORα3 transcripts are exclusively detected in testis; and in the remaining tissues including the cerebellum there is a mixture of RORα1 and RORα4 transcripts (M.B.-A., unpublished results). In the central nervous system (CNS) RORα mRNA localizes to the cerebellar Purkinje cells (PCs), various thalamic nuclei, and, during development, to other brain areas (6, 7). To study the physiological role of this orphan receptor we generated RORα null-mutant mice by gene targeting. In the course of this work the genetic basis of the *staggerer* (*sg*) mutation in mouse was identified by positional cloning as a deletion in the RORα gene (8). The *sg* mutation abolishes the development of cerebellar PCs in a cell-autonomous fashion (9, 10). The resulting immature morphology and severe cerebellar ataxia (11–13) suggest an essential role of RORα in the terminal differentiation of these cells.

Here, we present data which prove that the lack of functional RORα causes a phenotype encompassing all the salient features of neurological mouse mutation *sg*. In addition, we show that expression of RORα is confined to the CNS, skin, and testis. Our study leads to the conclusion that the absence of RORα causes dramatic effects exclusively in the cerebellum but apparently impairs only mildly, if at all, the morphology and physiology of the remaining brain areas, skin, and testis.

MATERIALS AND METHODS

Targeting the RORα Locus. A 1.8-kb PCR-generated DNA fragment containing part of the exon encoding the second zinc finger of RORα and its 5′ flanking sequences was cloned into the pGN vector (14), via *Xba*I and *Sac*II, to fuse the RORα exon with the pGN's *lacZ* gene and eventually creating a RORα/β-glactosidase (β-gal) fusion. After sequencing of the insert a 1.8-kb thymidine kinase (tk) gene cassette was cloned into the *Xba*I site. Finally, a *Xho*I–*Not*I 6.5-kb DNA fragment derived from the RORα locus of 129/Ola mouse containing intron sequences downstream of the second zinc finger was introduced resulting in the targeting construct pRORa-koc-TK. *Not*I-linearized pRORa-koc-TK was electroporated into 129/Ola ES HM1 cells as described (15). Chimeric mice were mated with C57BL/6 mice and offspring were genotyped by Southern hybridization of tail DNA by using a DNA fragment derived from the RORα locus upstream of the 1.8 kb *Xba*I–*Sac*II DNA fragment as a probe. Genomic DNA was digested by using *Bam*HI and size separated in a 0.8% agarose gel.

Behavioral Tests. Motor capability tests were performed with groups of 2- to 4-month-old wild-type RORα (+/+), heterozygous RORα knockout (+/−), homozygous RORα knockout (−/−) littermate mice, and a group of age-matched homozygous *staggerer* mutant mice (*sg*/*sg*).

The publication costs of this article were defrayed in part by page charge payment. This article must therefore be hereby marked "*advertisement*" in accordance with 18 U.S.C. §1734 solely to indicate this fact.

Abbreviations: CF, climbing fiber; CNS, central nervous system; EPSC, excited postsynaptic current; PC, Purkinje cells; ROR, retinoid-related orphan receptor; *sg*, *staggerer*; β-gal, β-glactosidase; GABA, γ-aminobutyric acid.

¶To whom reprint requests should be addressed. e-mail: michael.becker-andré@serono.com.

Motor coordination test. The apparatus consisted of an experimental box (35 × 35 × 25 cm). Half a centimeter above the bottom of the box was a platform in which 36 holes, 2 cm in diameter and arranged in a 6 × 6 array, have been drilled. The animal was placed in the middle of the platform and the number of times it stumbled (one leg diving into a hole) was recorded. The test lasted 5 min. The stumbling frequency (number of stumbles/min) was calculated.

Hanging test. The muscular tone of the animal was measured by hanging it by its two anterior paws on a rod, 25 cm long, 3 mm in diameter, and located 1.5 m above a thick carpet to cushion its eventual fall. The time during which the animal kept hanging on the rod was recorded. Three trials spaced by a 3-min pause were performed and a mean score was calculated. The test was limited to 180 sec.

Equilibrium test: the nonrotated rod. The apparatus consisted of a wooden horizontal rod (50 cm long and 3 cm in diameter) covered with sticking plaster to increase roughness. It was located 80 cm above a landing platform covered with a thick sheet of soft plastic to cushion the eventual fall of the animals. The animal was placed on the middle of the rod, its body axis perpendicular to the longitudinal axis of the rod. The time the animal stayed on the rod was recorded. The trial was stopped when the animal fell or otherwise after 180 sec.

Motor learning test: the rotarod. The apparatus was the same as used for the equilibrium test. The animal was placed on the middle of the rod, its body axis perpendicular to the longitudinal axis of the rod and its head directed against the direction of rotation, so that the animal had to progress forward to maintain balance. Training consisted of 10 rotations per day at 5 rpm. We recorded how long the mice stayed on the rod and which strategy they used. The maximum score was 180 sec, because the test was limited to 3 min (16, 17). Two kinds of strategies were observed and quantified: walking and hanging. Motor synchronization learning was achieved if after 10 consecutive trials the animal managed to stay on the rod for 180 sec.

Morphological Analysis of the Cerebellum. Four ROR$\alpha^{-/-}$ mice, aged from 3 to 5 months, were used. Three of them were fixed by intracardiac perfusion with 4% paraformaldehyde in 0.12 M phosphate buffer (pH 7.4). Frozen frontal (two mice) and parasagittal (one mouse) sections were obtained and double immuno-labeled with mAb Q113 (immunoperoxidase) detecting zebrin I and rabbit polyclonal antibodies against calbindin (fluorescein isothiocyanate-conjugated) as described (18). The antibodies were respectively gifts from R. Hawkes (University of Calgary, Calgary, Canada) and E. M. Lawson (Cambridge Research Station, Cambridge, U.K.). The fourth mouse was perfused with glutaraldehyde and paraformaldehyde (both at 1%), postfixed in osmium tetroxide, and embedded in Araldite. For light microscopy, 1-μm-thick parasagittal sections were stained with toluidine-blue. For electron microscopical analysis ultra-thin sections were either stained with lead citrate or immuno-stained with rabbit polyclonal anti-γ-aminobutyric acid (GABA) antibodies (Immunotech, Luminy, France) according to the postembedding immunogold method as described (19). The cerebella of a wild-type ROR$\alpha^{+/+}$ and a homozygous *sg/sg* mouse were also double immuno-stained with anti-zebrin I and anti-calbindin antibodies.

Electrophysiological Characterization of Cerebellar PCs. Sagittal slices, 250–300 μm thick, were prepared from the vermis of the cerebellum of 1- to 4-month-old ROR$\alpha^{-/-}$ and wild-type mice as described (20).

Histological Staining. Tissue was frozen in 2-methylbutane at −40°C for 5–10 min and stored at −80°C. Cryosections were cut (14 μm), air-dried on glass slides (Menzel, Braunschweig, Germany), fixed in 0.05% glutaraldehyde for 5 min at room temperature, washed with PBS, and incubated overnight at 37°C in PBS containing 4 mM $MgCl_2$, 2 mM $K_4Fe(CN)_6$, 2 mM $K_3Fe(CN)_6$, and 0.4 mg/ml 5-bromo-4-chloro-3-indolyl β-D-galactoside (X-Gal). After washing with PBS the section were counterstained (optional) with hematoxylin/eosin and mounted.

RESULTS

Generation of Mice Lacking RORα. We have generated mice lacking a functional RORα gene by using a targeting vector in which a β-gal gene replaced the second zinc finger of the DNA-binding domain of RORα. After homologous recombination the targeted gene encoded a fusion protein composed of RORα's N-terminal domain and first zinc finger followed by β-gal (Fig. 1*A*). Cross-breeding of heterozygous ROR$\alpha^{+/-}$ mice yielded homozygous null-mutant ROR$\alpha^{-/-}$ animals at the expected frequency of 25% as analyzed by genotyping (Fig. 1*B*) and easily identified by their ataxic behavior. About half of the ROR$\alpha^{-/-}$ mice died shortly after weaning whereas the remaining reached adulthood and showed normal life expectancy.

RORα Null-Mutant Mice Display Motor Deficits Nearly Identical to *staggerer* Mice. Global observation of ROR$\alpha^{-/-}$ mice show that they exhibit a paw clasping response and a strong ataxia similar to homozygous mutant *sg/sg* mice (21). To assess the motor capabilities of ROR$\alpha^{-/-}$ mice and to compare with *sg/sg* mice we quantified three parameters: the stumbling frequency, which is an indicator of the motor coordination ability; the hanging time, which indicates the degree of muscular strength; and the equilibrium capabilities. Stumbling frequency of *sg/sg* mice and ROR$\alpha^{-/-}$ mice is higher than that of wild-type littermates, whereas hanging and equilibrium times are significantly lower (Table 1). These results demonstrate that both ROR$\alpha^{-/-}$ and *sg/sg* mice suffer from motor coordination, hanging and equilibrium deficits (21, 22). However, *sg/sg* mice had lower scores in the equilibrium and hanging time tests than ROR$\alpha^{-/-}$ mice (Table 1). In the motor learning test with the rotarod, ROR$\alpha^{+/+}$ littermates and heterozygous ROR$\alpha^{+/-}$ mice reached the maximal score of 180 sec easily in the first trial (Fig. 2*A*) by exclusively using a walking strategy (Fig. 2*B*). In contrast, ROR$\alpha^{-/-}$ mice and *sg/sg*

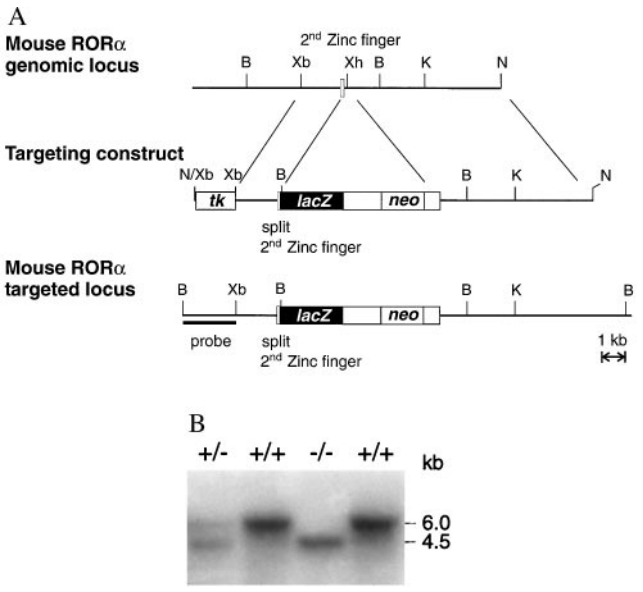

FIG. 1. Targeting the mouse RORα locus. (*A*) Schematic representation of the wild-type RORα locus, targeting vector, and recombined locus. In the targeted locus the exon of the second zinc finger of the DNA binding domain (filled box) is disrupted and fused to *lacZ* encoding β-gal. (*B*) Diagnostic Southern blot hybridization was performed by using the probe indicated in *A*. Lanes are homozygous (−/−), heterozygous (+/−), and wild-type (+/+) DNA.

Table 1. Quantification of equilibrium, motor coordination, and muscular strength of four groups of mice: wildtype (+/+), heterozygous RORα knockout (+/−), homozygous RORα knockout (−/−), and homozygous *sg/sg* mice

	+/+ (n = 14)	+/− (n = 14)	−/− (n = 13)	*sg/sg* (n =8)
Equilibrium time, sec	180 ± 0	180 ± 0	75 ± 23*	13 ± 2**
Stumbling frequency, no. of stumbling/min	0.3 ± 0.05	2.4 ± 0.4	6.0 ± 0.1*	12 ± 0.4*
Hanging time, sec	170 ± 10	160 ± 11	77 ± 21*	12 ± 4**

Scores are given as mean ± SEM. One asterisk represents a statistical difference ($P < 0.01$) to wild-type and heterozygous mice (Mann–Whitney test); two asterisks indicate a statistical difference to wild-type, homozygous, and heterozygous RORα knockout mice.

mice did not reach the maximal score, even after 10 days of training (Fig. 2*A*), and they used principally a hanging strategy to stay on the rotarod (Fig. 2*B*). Thus, ROR$\alpha^{-/-}$ and *sg/sg* mice are incapable of motor synchronization learning (23, 24). However, although *sg/sg* mice did not improve their score, ROR$\alpha^{-/-}$ mice improved significantly during the 10 test days.

Anatomical Characterization of the ROR$\alpha^{-/-}$ Cerebellum Reveals Identical Phenocopy of *staggerer*. In adult mutants the cerebellum is greatly reduced in size, particularly the intermediate region. The cytoarchitecture of the cortex is grossly altered: The molecular layer is very thin, PCs are not arranged in a monolayer (Fig. 3 *A* and *D*), the granular layer is almost nonexistent and depleted of granule cells. Studies with immunomarkers to visualize either all PCs or PC compartmentation have shown that their dendrites are smaller than normal, not confined to a single plane, and devoid of spiny branchlets (Fig. 3*D*). Moreover, zebrin I-immunostained PCs, present in wild-type ROR$\alpha^{+/+}$ cerebellum (Fig. 3*C*), are lacking in the mutant. Thus, the phenotype resembles that of *staggerer* cerebellum (Fig. 3*B*).

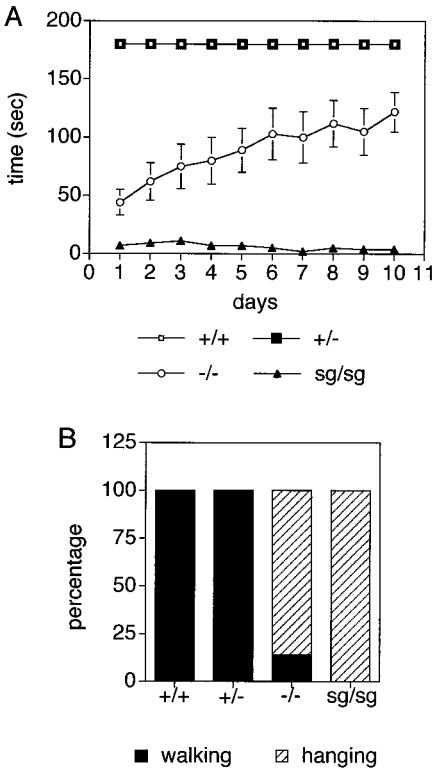

FIG. 2. Comparison of physical performance of ROR$\alpha^{-/-}$ and *staggerer* mice in the motor synchronization learning (rotarod) test. (*A*) Duration the mice stayed on the rotarod. Wild-type (+/+) (n = 10) and heterozygous RORα knockout mice (+/−) (n = 10) managed to stay on the rod for the entire 180 sec; homozygous RORα knockout mice (−/−) and *sg/sg* mice never reached this maximal score (n = 12). However, the ROR$\alpha^{-/-}$ mice significantly improved from day 1 to day 10 (Mann–Whitney, $P > 0.05$), whereas the *sg/sg* mice did not at all. (*B*) Strategy used by mice to stay on the rod. Wild-type (n = 10) and ROR$\alpha^{+/-}$ mice (n = 10) used exclusively walking, whereas ROR$\alpha^{-/-}$ mice and *sg/sg* mice (n = 12) used principally or exclusively hanging, respectively.

The electron microscopy analysis has corroborated the lack of granule cells. The subpial region solely contains reactive astrocytic processes. The molecular layer neuropil contains dispersed synaptic islands and tiny bundles of parallel fibers, both encapsulated by various layers of thin astrocytic processes. The majority of the axon terminals are GABA-immunoreactive (Fig. 3*E*), and some of them are GABA-negative and exhibit the features of parallel fiber varicosities (data not shown). Many PC bodies retain their immature somatic spines which remain postsynaptic to climbing fiber (CF) varicosities (Fig. 3*F*). However, CF translocation, although only partial, has occurred in the ROR$\alpha^{-/-}$ cerebellum because some of the stem dendrites have spines synaptically contacted by CF varicosities (data not shown). The inhibitory synaptic investment of mutant PCs is also altered. Although axon terminals resembling basket cell axons occur (Fig. 3*F*), they are rare, smaller than in control cerebellum, and do not establish characteristic pinceaux formations around the initial segment of PC axons (data not shown). Nevertheless, PC perikarya receive inhibitory synaptic inputs, as revealed with GABA immunocytochemistry (data not shown). Although PC perikarya abut the white matter axes of the folia, in the deeper third of the cortical gray matter mossy fiber profiles are numerous. The latter only occasionally form typical glomeruli of the simplest type because the large majority of the mossy fibers either only contact a few granule cell dendrites (Fig. 3*G*) or remain completely surrounded by astrocytic processes.

Cerebellar PCs of ROR$\alpha^{-/-}$ Mice Display Electrophysiological Characteristics Identical to those of *staggerer* Mice. Previous studies (12, 13) have established that cerebella from adult *sg/sg* mice are characterized by the multiple innervation of PCs by CFs, a feature normally only observed during the first 2 postnatal weeks (13, 25).

In keeping with previous observations (20), stimulation of the granular layer evoked typical all-or-none CF-mediated excited postsynaptic currents (EPSCs) (26) in 10 control brain PCs as tested in the voltage-clamp mode (Fig. 4*A1*). In the current-clamp mode, these responses consisted of an initial full spike followed by a plateau of depolarization with superimposed partial spikes, as in normal PCs (Fig. 4*A2*). In contrast, in all nine ROR$\alpha^{-/-}$ PCs recorded the evoked CF-EPSCs exhibited two to four steps (2.8 on average) in amplitude when the stimulus intensity was progressively increased (Fig. 4 *B1*, *B2*, and *C1*). This stepwise variation in amplitude was observed when cells were maintained at −80 mV as well as when they were held at −10 mV or −20 mV, to inactivate sodium and calcium voltage-dependent conductance. In the latter case the ratio of the amplitude of the two steps of the CF-EPSCs was the same as that measured at −80 mV (data not shown). Yet mean rise times and mean amplitudes of the largest step of these graded CF-mediated EPSCs were not significantly different from those observed in all-or-none responses in both mutant and wild-type mice. Finally, in the current-

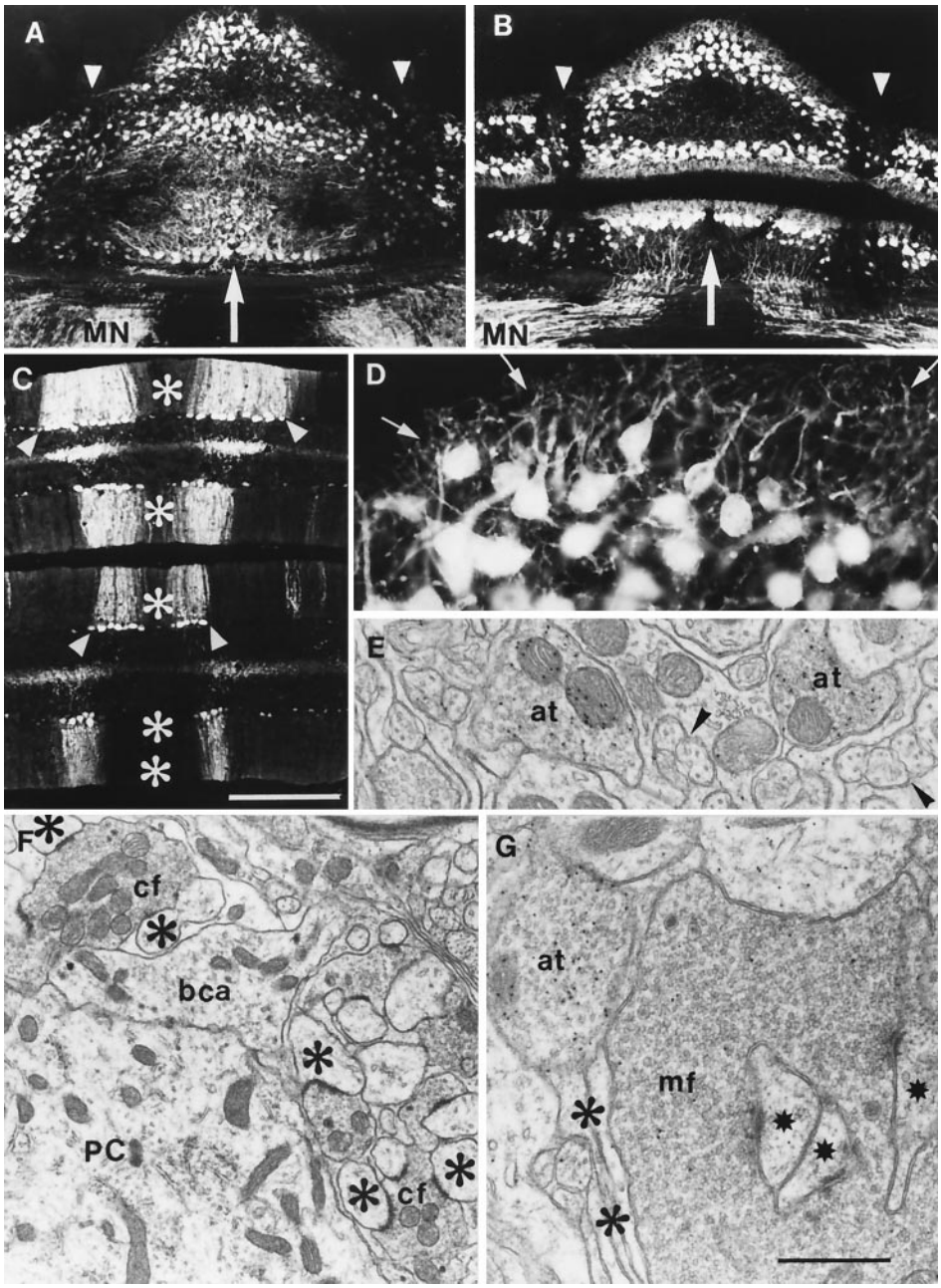

FIG. 3. Comparison of cellular phenotypes in ROR$\alpha^{-/-}$ (*A* and *D*), *sg*/*sg* (*B*), and ROR$\alpha^{+/+}$ mice (*C*) with double-immunolabeled preparations (zebrin I/calbindin). In frontal sections of ROR$\alpha^{-/-}$ (*A*) and *sg*/*sg* mice (*B*) the cerebellar phenotype is identical: the vermis is atrophic but lobulated (large arrows point to the midline), with disorganized PC bodies and thin molecular layer. Note that the immunostained PC projections are densely packed in the medial cerebellar nucleus (MN). All PCs are devoid of zebrin I because the narrow zones marked by arrowheads do not represent zebrin I-positive bands but zones of PC depletion. In contrast, in the ROR$\alpha^{+/+}$ cerebellum (*C*) PCs are arranged in a monolayer at the interface of the granular and molecular layers (arrowheads). The molecular layer is thick and contains the parasagittally oriented PC dendrites. Moreover, zebrin I-positive PCs (dark areas caused by quenching of the calbindin immunofluorescence by the immunoprecipitate) are confined to regularly occurring parasagittal bands (the central band is marked by asterisks). (*D*) High magnification of calbindin-positive PCs in the ROR$\alpha^{-/-}$ vermal cortex. Most of these neurons have apical dendrites that branch into small disoriented dendritic arbors (arrows). (*E–G*) Electron micrographs illustrating some features of the synaptic arrangement in the ROR$\alpha^{-/-}$ cerebellum. (*E*) High magnification of the molecular layer neuropil, in a preparation immunostained with anti-GABA antibodies, showing two immunogold-labeled axon terminals (at) apposed to small dendritic profiles. Parallel fibers, isolated or forming small clusters (arrowheads), are present in the layer. (*F*) Purkinje cell perikaryon (PC). Numerous perikaryal spines (asterisks) are postsynaptic to two axon terminals belonging to climbing fiber varicosities (cf) that have retained their immature pericellular nest location. A large terminal, probably belonging to a basket cell axon (bca), is apposed to the PC between the two climbing fiber varicosities. (*G*) Granular layer. A mossy fiber rosette (mf) is mostly surrounded by thin astrocytic processes (asterisks), and a few granule cell dendrites (stars). Note the immunogold, GABA-labeled axon terminal (at) almost directly apposed to the mossy fiber, testifying that most granule cell dendrites have disappeared. This terminal belongs to the Golgi cell axon. [Immunofluorescence, bar = 350 μm (*A–C*) and 70 μm (*D*); electron microscopy, bar = 0.6 μm (*E* and *G*) and 1.3 μm (*F*).]

clamp mode the largest step of the CF responses recorded at −70 mV from the nine multiply innervated cells was very similar to that of CF responses recorded in *sg*/*sg* mice (12, 13) (Fig. 4*A2*).

High Resolution Mapping of RORα Distribution: Confirmations and Surprises. Adult heterozygous RORα mutant (ROR$\alpha^{+/-}$) mice were examined for the distribution of β-gal activity indicative of RORα protein expression in various

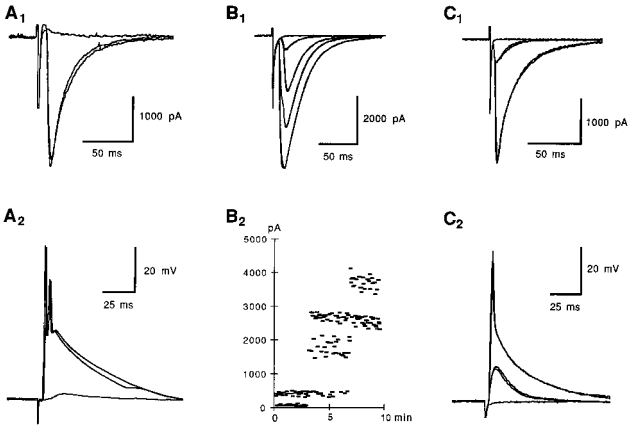

FIG. 4. Electrophysiological characterization of ROR$\alpha^{-/-}$ PCs. (*A1*) Two superimposed sweeps of all-or-none CF-mediated EPSCs in normal PCs and one subthreshold response evoked by stimulation of the granular layer at the holding potential of −80 mV. (*A2*) Same cell recorded in current-clamp mode at −70 mV. (*B1*) Superimposed sweeps of CF-mediated EPSCs elicited in a multiply innervated ROR$\alpha^{-/-}$ PC held at −80 mV by stimulating the granular layer with progressively increasing strength. (*B2*) Plot of amplitudes against time of CF-mediated EPSCs recorded at −80 mV in the same cell as in *B1*. Note the stepwise variation of the responses with progressively increasing stimulation strength. (*C1*) Same as in *B1* using another neuron. (*C2*) The cell was held in current-clamp mode at −80 mV and the granular layer was stimulated with progressively increasing intensity.

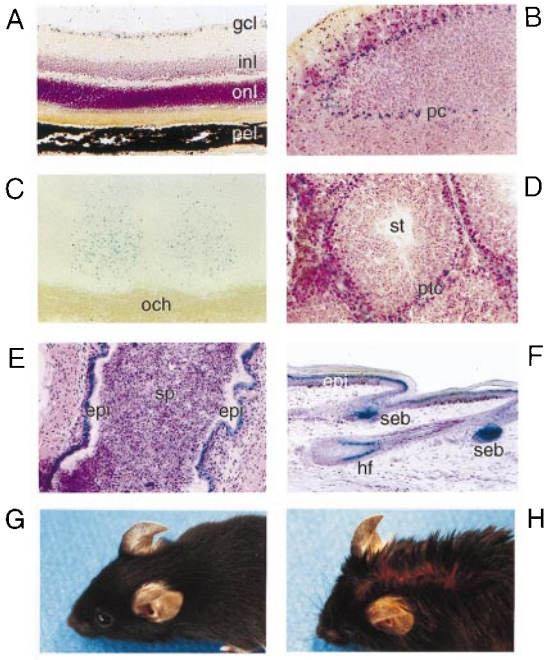

FIG. 5. (*A–F*) Expression of RORα revealed by β-gal activity in ROR$\alpha^{+/-}$ mice. Tissue sections were stained with the β-gal substrate 5-bromo-4-chloro-3-indolyl β-D-galactoside (X-Gal) (*C*) or additionally counterstained with either cresylviolet (*A, B, D,* and *F*) or hematoxylin/eosin (*E*). (*A*) Retina; gcl, ganglion cells; inl, inner nuclear layer; onl, outer nuclear layer; pel, pigment epithelium layer. (*B*) Cerebellum; pc, Purkinje cells. (*C*) Suprachiasmatic nuclei; och, optic chiasm. (*D*) Testis; ptc, peritubular cells; st, seminiferous tubule. (*E*) Epididymis; sp, spermatocytes; epi, epithelium. (*F*) Tail skin; epi, epidermis; seb, sebaceous gland; hf, hair follicle. (*G* and *H*) Comparison of a ROR$\alpha^{+/-}$ and a ROR$\alpha^{-/-}$ mouse; note the difference in the appearance of the fur and the partially exposed skin of the ROR$\alpha^{-/-}$ mouse (*H*).

tissues. As expected, enzyme activity was found in various areas of the brain including retinal ganglion cells, cerebellar PCs (Fig. 5 *A* and *B*) and some nuclei of the thalamus (data not shown). Moreover, our data show that RORα is also expressed in the suprachiasmatic nuclei of the hypothalamus, the testis, and skin (Fig. 5 *C–F*). To our surprise, other organs such as liver, heart, spleen, lung, and leukocytes, which have been shown to express significant to high levels of RORα mRNA (2, 27), did not display any detectable enzyme activity. The same expression profile was observed in the respective ROR$\alpha^{-/-}$ tissues—with the exception of the cerebellar PCs in which the RORα/β-gal fusion product is only scarcely expressed (data not shown).

RORα expression was observed in testis only after sexual maturation and specifically localized to peritubular cells (Fig. 5*D*). In addition, and already before puberty, massive expression of RORα was detected in the epithelial cell layer of the epididymis (Fig. 5*E*). Yet in the knockout as well as in the *sg/sg* mice we observed no abnormal phenotype, i.e., the animals produced spermatocytes and were putatively fertile (22).

In skin, β-gal activity localized to the epidermis, the hair follicle, and the sebaceous gland (Fig. 5*F*). In the epidermis RORα is expressed in suprabasal differentiating keratinocytes but not in proliferating keratinocytes of the basal generative compartment. In the growing (anagen) hair follicle, expression of RORα is confined to a discrete set of differentiating keratinocytes above the dividing cells of the hair matrix. This staining is absent from hair follicles in other hair cycle phases including the katagene, telogen, and early anagen phase (data not shown). In ROR$\alpha^{-/-}$ mice the anatomical and histological situation of the skin appears normal. However, the mice develop a fur that is significantly less dense lacking in particular most of the duvet hair (Fig. 5 *G* and *H*). When shaved, the hair grew back only very slowly (not shown). We observed a similar behavior with *sg/sg* mice. However, we also noticed that a rich and balanced nourishment mitigates this phenotype.

DISCUSSION

The phenotype of the ROR$\alpha^{-/-}$ mice proves that the *staggerer* mutation is based on the functional disruption of the nuclear receptor RORα gene (8). ROR$\alpha^{-/-}$ and *sg/sg* mice exhibit the same disorders, i.e., ataxia and motor capability deficiencies. However, we also noted differences. ROR$\alpha^{-/-}$ mice are less asthenic, reached a better equilibrium score, and performed significantly better in the rotarod test than *sg/sg* mice. These discrepancies could be explained by the different genetic backgrounds of ROR$\alpha^{-/-}$ (C57BL/6, 129/Ola) and *sg/sg* mice (C57BL/6). Alternatively, the difference of the RORα gene mutations in the corresponding strains might be considered: in *sg/sg* mice the RORα gene is truncated at the level of the ligand binding domain leaving intact the DNA-binding domain of the encoded protein. Thus, expressed truncated *staggerer* RORα could still interact with its appropriate DNA binding sites but would be incapable of promoting transcription. Consequently, it could act as a dominant negative isoform and as such might exacerbate the mutant's phenotype. In contrast, in ROR$\alpha^{-/-}$ mice the RORα gene is disrupted at the level of the second zinc finger and the corresponding gene product is incompetent of binding to DNA.

The abnormal anatomical phenotype of the adult ROR$\alpha^{-/-}$ cerebellum also corresponds to that of the *staggerer* mouse (Fig. 3 *A* and *B*). In both, the cerebellum is agranular, PCs are ectopic, reduced in number, and exhibit atrophic cell bodies and dendritic trees that are devoid of most of their spines (9, 11, 28). Moreover, a prominent feature of the mammalian cerebellum is its organization into parasagittal compartments, characterized by the biochemical heterogeneity of their PCs. One marker of such compartments is zebrin (29) which is expressed by a subset of PCs confined to regularly occurring parasagittal bands. From all known cerebellar mutants preserving PCs into adulthood only the *staggerer* mouse lacks

zebrin I-positive PCs (30). The absence of zebrin I-immunoreactive PCs in the ROR$\alpha^{-/-}$ cerebellum convincingly shows that both mutations induce the same cerebellar phenotype. The analysis of the cerebellar synaptology of ROR$\alpha^{-/-}$ cerebellum further supports the conclusion that this cerebellum is the precise phenocopy of that of *staggerer*. The partial translocation of CFs from PC bodies to stem dendrites and the absence of pericellular nests and pinceaux formations emerging from basket cell axons which characterize the synaptic investment of PCs in the RORα null mutation are salient features of *staggerer* PCs (31–33). The occurrence in the null mutant of mossy fibers partially or even entirely denuded of their postsynaptic granule cell dendrites at the glomeruli reproduces the *staggerer* condition (11, 32). Finally, similar to the behavioral and anatomical data of this study, also the electrophysiological results reveal that *staggerer* mutation and RORα null mutation converge on the same phenotype. Taken together, the comparative description of the phenotype of ROR$\alpha^{-/-}$ and *sg/sg* mice ultimately proves that both mutations cause a nearly identical cerebellar phenotype by affecting the same gene.

We established a high-resolution RORα protein expression map by using the *lacZ* reporter gene fused to the RORα gene locus. Within the CNS the expression pattern fits well with the mRNA distribution pattern based on *in situ* hybridization data (6, 7). In addition, we found expression in retinal ganglion cells and in the suprachiasmatic nuclei, the central part of the mammalian circadian timing system. Interestingly, there exists a report describing an arrhythmic feeding behavior in *sg/sg* mice (34). A careful analysis of *sg/sg* or ROR$\alpha^{-/-}$ mice with respect to their circadian behavior might reveal significant abnormalities in the biological timing system. In the periphery, RORα protein is expressed at detectable levels only in skin and testis. This is surprising in view of the distribution pattern of RORα mRNA (2, 27). In particular, peripheral blood leukocytes (T cells, B cells, neutrophils) containing highest amounts of RORα mRNA second to skin (M.B.-A., unpublished data) were negative in the β-gal assay. We hypothesize that RORα expression in those cells and tissues could be controlled at the level of translation obeying to developmental and/or physiological signals, such as apoptosis and tissue-specific differentiation programs. In *sg/sg* mice a delay in terminating immune responses was observed (35), suggesting a defect in regulatory feedback mechanisms caused by the lack of RORα, possibly involving macrophages (36).

The absence of RORα causes massive PC loss leading to impaired development of the cerebellum. Apparently, RORα serves vital functions for proper maturation of these cells. The regenerative growth deficiency of the pelage hair of ROR$\alpha^{-/-}$ mice suggests that RORα also plays an important role in terminal differentiation processes of this skin appendix. Although the lack of RORα in cerebellar PCs and in keratinocytes of adult hair follicles has clear effects, the role of RORα in epidermal keratinocytes, sebaceous gland, retina, thalamus, and testis is less obvious. There, RORα might be involved in the fine-tuning of physiological processes rather than in bringing about developmental events. Alternatively, it is conceivable that the lack of RORα in these tissues is neutralized by compensatory mechanisms during the development. The identification of genes regulated by RORα (37) will be one of the next crucial steps toward a better understanding of the mechanism of action of this orphan nuclear receptor. To this end the corresponding null-mutant animals will be of great utility.

We thank Drs. Jonathan K. C. Knowles and John F. DeLamarter for their enthusiastic support, Chris Hebert for photographical assistance, Denise Gretener for technical assistance, Laurent Potier and Roberto Lia for the animal work, and Dr. Jean-François Nicholas for helpful discussions.

1. Evans, R. M. (1988) *Science* **240,** 889–895.
2. Becker-André, M., André, E. & DeLamarter, J. F. (1993) *Biochem. Biophys. Res. Commun.* **194,** 1371–1379.
3. Giguère, V., Tini, M., Flock, G., Ong, E., Evans, R. M. & Otulakowski, G. (1994) *Genes Dev.* **8,** 538–553.
4. Carlberg, C., Hooft van Hujisdujinen, R., Staple, J. K., DeLamarter, J. F. & Becker-André, M. (1994) *Mol. Endocrinol.* **8,** 757–770.
5. Hirose, T., Smith, R. J. & Jetten, A. M. (1994) *Biochem. Biophys. Res. Commun.* **205,** 1976–1983.
6. Matsui, T., Sashihara, S., Oh, Y. & Waxman, S. G. (1995) *Mol. Brain Res.* **33,** 217–226.
7. Sashihara, S., Felts, P. A., Waxman, S. G. & Matsui, T. (1996) *Mol. Brain Res.* **42,** 109–117.
8. Hamilton, B. A., Frankel, W. N., Kerrebrock, A. W., Hawkins, T. L., FitzHugh, W., *et al.* (1996) *Nature (London)* **379,** 736–739.
9. Sidmann, R. L., Lane, P. W. & Dickie, M. M. (1962) *Science* **137,** 610–612.
10. Herrup, K. & Mullen, R. J. (1979) *Brain Res.* **67,** 443–457.
11. Sotelo, C. & Changeux, J. P. (1974) *Brain Res.* **67,** 519–526.
12. Crépel, F., Delhaye-Bouchaud, N., Guatavino, J. M. & Sampaio, I. (1980) *Nature (London)* **283,** 483–484.
13. Mariani, J. & Changeux, J. P. (1980) *J. Neurobiol.* **11,** 41–50.
14. Le Mouellic, H., Lallemand, Y. & Brulet, P. (1990) *Proc. Natl. Acad. Sci. USA* **87,** 4712–4716.
15. Magin, T. & Melton, D. (1992) *Nucleic Acids Res.* **20,** 3795.
16. Auvray, N., Caston, J., Reber, A. & Steltz, T. (1989) *Brain Res.* **505,** 291–301.
17. Zion, C., Auvray, N., Caston, J., Reber, A. & Steltz, T. (1990) *Brain Res.* **515,** 104–110.
18. Rouse, R. V. & Sotelo, C. (1990) *Exp. Brain Res.* **82,** 401–407.
19. Angaut, P. & Sotelo, C. (1989) *Brain Res.* **479,** 361–365.
20. Conquet, F., Bashir, Z. I., Davies, C. H., Daniel, H., Ferraguti, F., Bordi, F., Franz–Bacon, K., Reggiani, A., Matarese, V., Conde, F., *et al*. (1994) *Nature (London)* **372,** 237–243.
21. Lalonde, R. (1987) *Exp. Brain Res.* **68,** 417–420.
22. Guastavino, J. M. (1984) *Physiol. Behav.* **32,** 225–228.
23. Lalonde, R., Bensoula, A. N. & Filali, M. (1995) *Neurosci. Res.* **22,** 423–426.
24. Caston, J., Delhaye-Bouchaud, N. & Mariani, J. (1996) *Behav. Brain Res.* **72,** 97–102.
25. Crépel, F., Delhaye-Bouchaud, N. & Dupont, J. L. (1981) *Dev. Brain Res.* **1,** 59–71.
26. Aiba, A., Kano, M., Chen, C., Stanton, M. E., Fox, G. D., Herrup, K., Zwingman, T. A. & Tonegawa, S. (1994) *Cell* **79,** 377–388.
27. Forman, B. M., Chen, J., Blumberg, B., Kliewer, S. A., Henshaw, R., Ong, E. S. & Evans, R. M. (1994) *Mol. Endocrinol.* **8,** 1253–1261.
28. Herrup, K. & Mullen, R. J. (1981) *Dev. Brain Res.* **1,** 475–485.
29. Hawkes, R. & Leclerc, N. J. (1986) *J. Comp. Neurol.* **244,** 481–491.
30. Sotelo, C. & Wassef, M. (1991) *Soc. Neurosci. Abst.* **17,** 918.
31. Sotelo, C. (1975) in *Physiology and Pathology of Dendrites*, ed. Kreuzberg, G. W. (Raven, New York), Vol. 12, 335–351.
32. Landis, D. M. D. & Sidman, R. L. (1978) *J. Comp. Neurol.* **179,** 831–864.
33. Sotelo, C. (1990) *J. Exp. Biol.* **153,** 225–249.
34. Guastavino, J. M., Bertin, R. & Portet, R. (1991) *Physiol. Behav.* **49,** 405–409.
35. Trenkner, E. & Hoffmann, M. K. (1986) *J. Neurosci.* **6,** 1733–1737.
36. Kopmels, B., Mariani, J., Delhaye-Bouchaud, N., Audibert, F., Fradelizi, D. & Wollman, E. E. (1992) *J. Neurochem.* **58,** 192–199.
37. Vu-Dac, N., Gervois, P., Grotzinger, T., De Vos, P., Schoonjans, K., Fruchart, J. C., Auwerx, J., Mariani, J., Tedgui, A. & Staels, B. (1997) *J. Biol. Chem.* **272,** 22401–22404.